Available online at www.sciencedirect.com

SciVerse ScienceDirect

Ceramics International 38 (2012) 5251–5255

CERAMICS INTERNATIONAL

www.elsevier.com/locate/ceramint

Electrical properties of germanium oxide with α-quartz structure prepared by chemical precipitation

C.V. Ramana [a,*], I.B. Troitskaia [b], S.A. Gromilov [c], V.V. Atuchin [b]

[a] Department of Mechanical Engineering, University of Texas at El Paso, El Paso, TX 79968, USA
[b] Laboratory of Optical Materials and Structures, Institute of Semiconductor Physics, SB RAS, Novosibirsk 630090, Russia
[c] Laboratory of Crystal Chemistry, Institute of Inorganic Chemistry, SB RAS, Novosibirsk 630090, Russia

Received 15 February 2012; received in revised form 7 March 2012; accepted 13 March 2012
Available online 31 March 2012

Abstract

Germanium dioxide (GeO_2) crystals were prepared by a chemical precipitation method at a relatively low-temperature (100 °C). The structure and electrical properties of the grown GeO_2 crystals were evaluated. GeO_2 crystals exhibit α-quartz type crystal structure with lattice parameters: $a = 4.987(4)$ Å and $c = 5.652(5)$ Å. DC conductivity variation measured in the temperature range of 120–300 K reveals the dielectric behavior of the GeO_2 crystals. The temperature dependent electrical conductivity curves exhibit two distinct regions indicative of two different types of electrical transport mechanisms. Analysis of the conductivity indicates that the small polaron and variable-range-hopping mechanisms are operative in 180–300 K and 120–180 K temperature regions, respectively.

Keywords: C. Electrical conductivity; GeO_2; Crystal structure

1. Introduction

The growth, characterization, and utilization of metal-oxide crystals for application in modern electronic and optical devices continue to be an interesting topic for theoretical and experimental investigations. Germanium dioxide (GeO_2) exhibits many interesting physicochemical properties for applications in optical, electronic and optoelectronic devices [1–15]. GeO_2 is a photoluminescence and dielectric material. It exhibits high values of dielectric constant, refractive index, thermal stability and mechanical strength. Photo-sensor capability of GeO_2 has been confirmed by optical spectroscopic methods such as Raman-spectroscopy and electron spin resonance spectroscopy coupled with structural measurements [1–3]. Due to these fascinating optical and electronic properties, GeO_2 has been considered as a promising material for optical waveguides and nano-connections in optoelectronic communications.

Synthesis and optimization of a particular phase of GeO_2 crystals is very important as this material exhibits several polymorphs [15–21]. The tetragonal α-phase with rutile type structure ($P4_2/mnm$, PDF 35-729 [15,16]), in which Ge is six-fold coordinated, is stable up to 1047 °C. The trigonal/rhombohedral β-phase with α-quartz type [17–20] ($P3_121$, PDF 04-498 [17,18] and $P3_221$, PDF 36-1463 [19,20]), in which Ge is four-fold coordinated, is stable above 1035 °C. Several high-pressure phases and glassy structures of GeO_2 were also reported in the literature [21]. GeO_2 crystals are usually produced by either physical evaporation or thermal oxidation methods. Crystallization through these techniques leads to the formation of one-dimensional structures [4–7]. Attempts were made to obtain the nanofibers by electrospinning process [8]. The GeO_2 whiskers were fabricated by ablating Ge target at $T = 820$ °C with a pulsed KrF excimer laser in an argon atmosphere [9]. Chemical precipitation and hydrothermal methods were also employed to grow three-dimensional GeO_2 structures with sizes from 15 nm to several centimeters depending on synthesis conditions [10–13]. Wang et al. have studied the ion-irradiation induced polymorphs of GeO_2 [22]. Hexagonal α-phase GeO_2 crystal formation on the Ge single crystal surfaces due to acid vapor exposure was reported by

* Corresponding author. +1 9157478690.
E-mail address: rvchintalapalle@utep.edu (C.V. Ramana).

0272-8842/$36.00
doi:10.1016/j.ceramint.2012.03.035

Kalem et al. [23]. Kim at el. demonstrated the growth of uncommon cone-shaped structures of GeO_2 using a thermal evaporation process [14]. In present study we investigate the β-phase GeO_2 crystals with α-quartz type structure grown using a low-temperature ($T = 100 \pm 5\ ^\circ C$) chemical precipitation method. Specifically, the electrical properties of β-phase GeO_2 crystals with α-quartz type structure are reported for the first time in this article.

2. Materials and methods

The starting materials were GeO_2 powder (Umicore Electro-optic Materials) with optical grade, aqueous ammonia (20.27 wt.%), nitric acid (69.23 wt.%) and distilled water. Two steps were carried out to obtain a GeO_2 precipitate. At first 0.2 g of GeO_2 was added to 50 ml distilled water and heated under magnetic stirring to a temperature of 90 °C. Then 1.6 ml aqueous ammonia was slowly added into the solution to form an ammonium germanate aqua solution with a pH = 10 and germanium concentration $C_{Ge} = 0.038$ mol/l. Under the above conditions the reaction between crystalline GeO_2 and aqueous ammonia produces germanate ions as monomers [24,25]. At second stage, 5 ml nitric acid was added to ammonium germanate solution and white precipitate appeared when the solution was evaporated down to 10 ml volume. The precipitate obtained was separated by centrifugation and washed with distilled water several times to pH = 6 of washing water. The final product was dried in air at 80 °C.

Structural properties of germanium oxide were evaluated with X-ray diffraction (XRD) analysis. XRD patterns were recorded by DRON-3M device with Cu Kα radiation, Ni filter, counting 10 s per step, step size 0.02°. The microstructure and morphology of GeO_2 nanocrystals was determined by scanning electron microscopy (SEM) using the Hitachi S4800 high-performance machine. The secondary electron imaging was employed to obtain the images. DC electrical resistivity measurements were carried out under the vacuum of 10^{-2} Torr by two-probe method in the temperature range 120–300 K employing a closed cycle refrigerator (CCR). Resistance was measured by employing a Keithley electrometer (Keithley 6517A Electrometer/High resistance meter). The temperature was measured using a silicon diode sensor and employing a Lakeshore temperature controller (Model No. 330). Compressed sample was used for electrical measurements. A pressure of 5 tons is applied to make a pellet of 10 mm diameter.

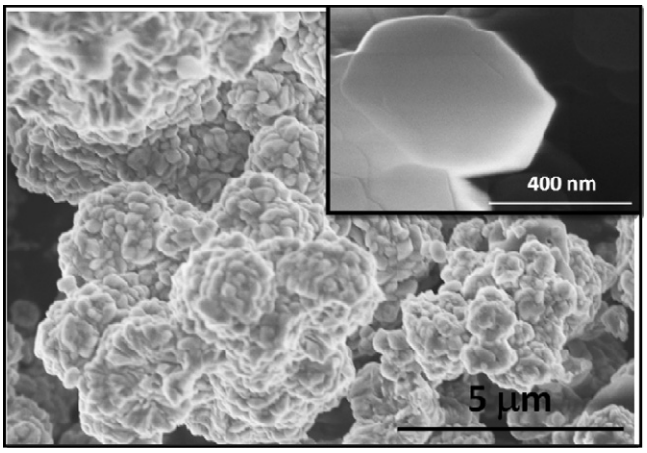

Fig. 1. SEM image of the GeO_2 precipitate onto silicon substrate.

3. Results and discussion

The micromorphology of final product deposited onto silicon substrate is shown in Fig. 1. The powder is formed by uniform non-facetted particles with diameter of ~0.5 μm, which is also confirmed by the X-ray diffraction studies. Inset of Fig. 1 shows a typical particle imaged at further high

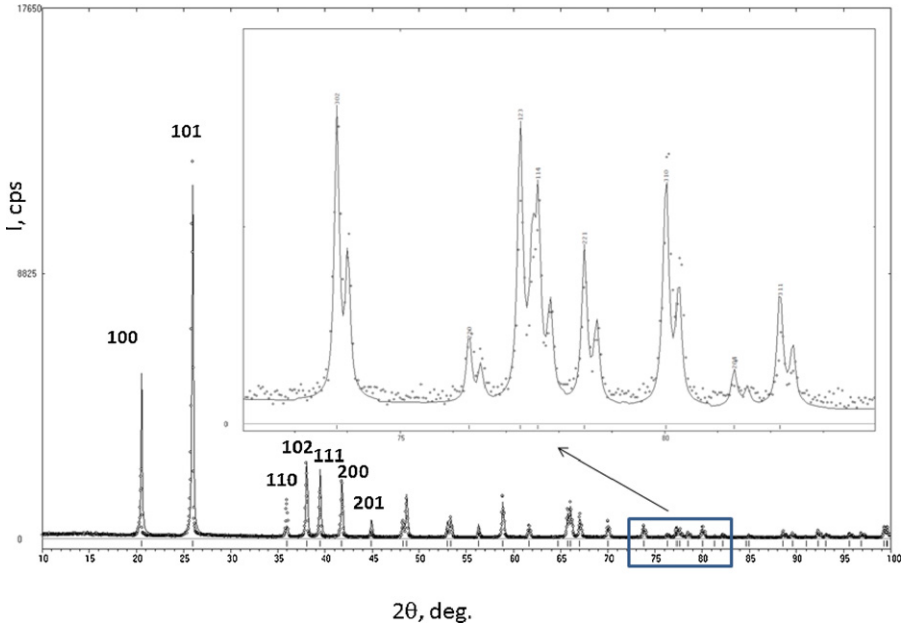

Fig. 2. X-ray diffraction pattern of the β-GeO_2 sample.

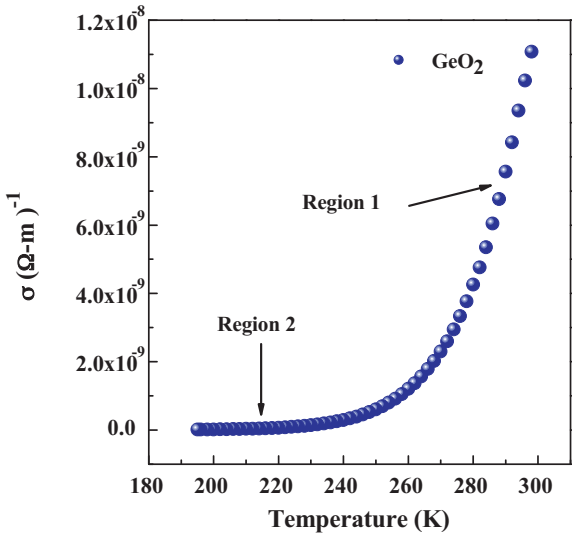

Fig. 3. DC electrical conductivity variation of GeO_2 with temperature.

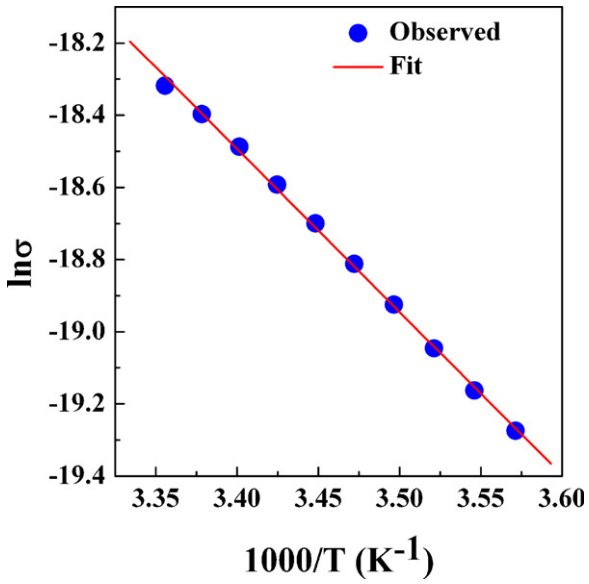

Fig. 4. The relation between ln σ T and 1000/T for β-GeO_2 crystals.

magnification. The particles possess strong charging effect under electron beam illumination. In Fig. 2, the XRD pattern is shown. All the diffraction peaks were successfully indexed and their positions are in good agreement with those of trigonal β-GeO_2, space group $P3_221$. As it is shown in the insert, at higher 2θ angles the Kα doublets are well resolved that verifies excellent crystallinity of the precipitate. The full-profile refinement gives the cell parameters $a = 4.987(4)$ Å and $c = 5.652(5)$ Å that is in good relation with earlier results available for β-GeO_2 [16,18].

The variation of DC electrical conductivity of GeO_2 is shown in Fig. 3. Electrical conductivity decreases exponentially with decreasing the temperature from 300 K to 180 K which is characteristic of either semiconducting or insulating nature of the material. Conductivity in oxides is due to both hopping of electrons and charge transport *via* excited states and it can be expressed as [26–29]:

$$\sigma = A_1 \exp\left(\frac{-E_1}{k_B T}\right) + A_2 \exp\left(\frac{-E_2}{k_B T}\right) + A_3 \exp\left(\frac{-E_3}{k_B T}\right) + \cdots \quad (1)$$

where E_1 is the activation energy for intrinsic conduction and E_2, E_3, ... are the activation energies needed for hopping conduction. A_1, A_2, A_3 are constants and k_B is the Boltzmann constant.

It is evident from the electrical conductivity plot (Fig. 3) that two different slopes exists for GeO_2 crystals indicating that the conduction is through an activated process having two different conduction mechanisms. Activation energy values at different temperature ranges (300–260 K and 260–180 K) were calculated from the ln σ *vs.* 1000/T plot which are given in Table 1. Activation energy values were found to be higher at 300–260 K region (0.38 eV) and lower at 260–180 K region (0.13 eV). Decreasing activation energy with decreasing temperature has been explained by small-polaron theory [26,27]. The variable range hopping (VRH) model of small polarons also predicts continuously decreasing activation energy with decreasing temperature [26,27].

In order to obtain a clear distinction between the two conduction mechanisms (two different slopes in Fig. 3), both the models were taken into account to fit the electrical conductivity data, namely the small-polaron model and the VRH model [26,27]. In the temperature regime 260–300 K, the conductivity data can be interpreted in terms of the phonon-assisted hopping model given by Mott [28]:

$$\sigma = \frac{e^2 \nu_{ph} c(1-c)}{k_B T R} \exp(-2\alpha R) \exp\left(-\frac{E}{kT}\right) \quad (2)$$

where ν_{ph} is the optical phonon frequency, c is the fraction of reduced metal ions (the ratio of ion concentration in the low valence state to the total concentration of ions), R is the average spacing between the ions, α is the localization length and E is the activation energy. Fig. 4 shows the plot between ln σT and 1000/T. The parameters ν_{ph} is $\sim 10^{13}$, R and E are constants.

Table 1
Electrical parameters calculated for GeO_2 crystals produced by chemical precipitation method.

Compound	Activation energy (eV)		A (Ω^{-1} cm^{-1} K$^{1/2}$)	B (K$^{1/4}$)	$N(E_F)$ (eV^{-1} cm^{-3}) $\times 10^{19}$
	260–300 K	180–260 K			
GeO_2	0.38	0.13	27781	51.45	3.34

Assuming a strong electron–phonon interaction, it is proposed in Ref. [28] that

$$E = E_H + \frac{E_D}{2} \quad \text{for} \quad \left(\frac{T > \theta_D}{2}\right) \tag{3}$$

$$E = E_D \quad \text{for} \quad \left(\frac{T < \theta_D}{4}\right) \tag{4}$$

where E_H is the polaron hopping energy, E_D is the disorder energy arising from the energy difference of neighbors between two hopping sites and θ_D is the Debye temperature. The polaron radius can be calculated using the formula [27,29]:

$$r_p = \left(\frac{\pi}{6}\right)^{1/3}\left(\frac{R}{2}\right) \tag{5}$$

where R is the d spacing. Value of r_p was found to be 0.17 nm. The procedure suggested by Greaves as a modification of Mott's model of VRH could be applied in the second temperature region (180–260 K), where σ follows:

$$\sigma T^{1/2} = A\exp(-BT^{-1/4}) \tag{6}$$

where A and B are constants and B is expressed as

$$B = 2.1\left[\frac{\alpha^3}{k_B N(E_F)}\right]^{1/4} \tag{7}$$

$N(E_F)$ is the density of localized states at E_F and α^{-1} is the decay constant of the wave function of localized states at E_F. Variable range hopping model seems to be valid in the temperature range 160–220 K and a good fit of the experimental data to Eq. (6) is shown in Fig. 5 ($\ln(\sigma T^{1/2})$ *vs.* $T^{-1/4}$ plot). The parameters A and B calculated from this curve are presented in Table 1. The density of localized states at the Fermi level, $N(E_F)$, has been calculated taking a constant value of α^{-1} (10^{-7} cm). The determined value is $N(E_F) \sim 3.34 \times 10^{19}\ \text{eV}^{-1}\ \text{cm}^{-3}$. A good fit of the Mott's VRH model has been verified by calculating the hopping parameters and the Mott's requirements ($R_{hop}\alpha \geq 1$ and $E_{hop} > k_BT$). Here R_{Hop} and E_{hop} are temperature dependent hopping distance and average polaron hopping energy, respectively:

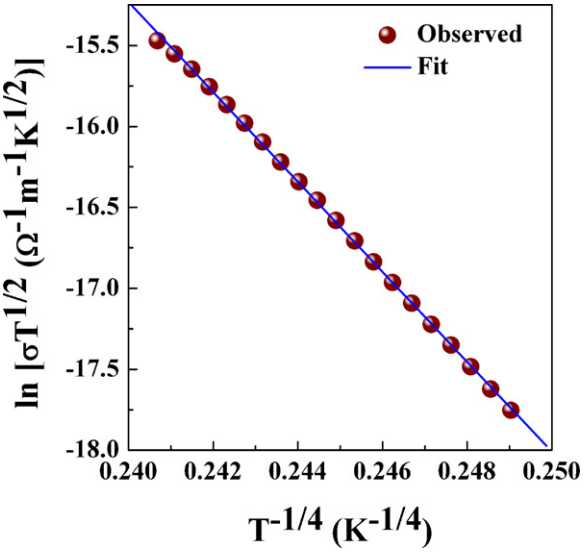

Fig. 5. The relation between $\ln(\sigma T^{1/2})$ and $T^{-1/4}$ for β-GeO_2 crystals.

$$R_{hop} = \left[\frac{9}{8\pi N(E_F)\alpha k_B T}\right]^{1/4} \tag{8}$$

$$E_{hop} = \frac{3}{4\pi R_{hop}^3 N(E_F)} \tag{9}$$

The calculated average values of R_{hop} and E_{hop} at 260 K for both the compounds are found to be 0.29 nm and 1.3 eV. The values of $R_{hop}\alpha$ and E_{hop} are found to be 2.9 and 1.3 eV, respectively. The requirements ($R_{hop}\alpha \geq 1$ and $E_{hop} > k_BT$) are clearly satisfied.

4. Conclusions

GeO_2 crystals were prepared by a chemical precipitation method at a relatively low-temperature of 100 °C. The structure analysis reveal that the GeO_2 crystals exhibit α-quartz type crystal structure with lattice parameters: $a = 4.987(4)$ Å and $c = 5.652(5)$ Å. The detailed electrical property analysis indicates that the DC conductivity variation in the temperature range of 120–300 K exhibits characteristic dielectric behavior of the GeO_2 crystals. The temperature dependent electrical conductivity behavior showed the two distinct regions indicative of the small polaron and variable-range-hopping mechanisms in electrical transport. The small polaron and variable range hopping mechanisms are operative in 180–300 K and 120–180 K temperature regions, respectively. The corresponding activation energies derived are 0.38 eV and 0.13 eV, respectively.

References

[1] N. Terakado, K. Tanaka, Photo-induced phenomena in GeO_2 glass, J. Non-Cryst. Solids 352 (2006) 3815–3822.
[2] N. Terakado, K. Tanaka, Photo-induced phenomena in sputtered GeO_2 films, J. Non-Cryst. Solids 351 (2005) 54–60.
[3] M. Zhou, L. Shao, L. Miao, Matrix isolation infrared spectroscopic and density functional theoretical calculations of the GeO_2^- and GeO_2^- anions, J. Phys. Chem. A 106 (2002) 6483–6486.
[4] Y. Su, X. Liang, S. Li, Y. Chen, Q. Zhou, S. Yin, X. Meng, M. Kong, Self-catalytic VLS growth and optical properties of single-crystalline GeO_2 nanowire arrays, Mater. Lett. 62 (2008) 1010–1013.
[5] H.W. Kim, J.W. Lee, GeO_2 nanostructures fabricated by heating of Ge powders: Pt-catalyzed growth, structure, and photoluminescence, Physica E 40 (2008) 2499–2503.
[6] Z. Jiang, T. Xie, G.J. Wang, X.Y. Yuan, C.H. Ye, W.P. Cai, G.W. Meng, G.H. Li, L.D. Zhang, GeO_2 nanotubes and nanorods synthesized by vapor phase reactions, Mater. Lett. 59 (2005) 416–419.
[7] P. Hidalgo, B. Méndez, J. Piqueras, GeO_2 nanowires and nanoneedles grown by thermal deposition without catalyst, Nanotechnology 16 (2005) 2521–2524.
[8] H.Y. Kim, P. Viswanathamurthi, N. Bhattarai, D.R. Lee, Preparation and morphology of germanium oxide nanofibers, Rev. Adv. Mater. Sci. 5 (2003) 220–223.
[9] Y.H. Tang, Y.F. Zhang, N. Wang, I. Bello, C.S. Lee, S.T. Lee, Germanium dioxide whiskers synthesized by laser ablation, Appl. Phys. Lett. 74 (1999) 3824–3826.

[10] X. Chen, Q. Cai, J. Zhang, Z. Chen, W. Wang, Z. Wu, Synthesis and growth of germanium oxide nanoparticles in AOT reversed micelle, Mater. Lett. 61 (2007) 535–537.
[11] C. Jing, J. Hou, Y. Zhang, Morphology controls of GeO_2 particles precipitated by a facile acid-induced decomposition of germanate ions in aqueous madium, J. Cryst. Growth 310 (2008) 391–396.
[12] D.V. Balitsky, V.S. Balitsky, D.Y. Pushcharovsky, G.V. Bondarenko, A.V. Kosenko, Growth and characterization of GeO_2 single crystals with the quartz structure, J. Cryst. Growth 180 (1997) 212–219.
[13] H.P. Wu, J.F. Liu, M.Y. Ge, L. Niu, Y.W. Zeng, Y.W. Wang, G.L. Lv, L.N. Wang, G.Q. Zhang, J.Z. Jiang, Preparation of monodisperse GeO_2 nanocubes in a reverse micelle system, Chem. Mater. 18 (2006) 1817–1820.
[14] H.W. Kim, S.H. Shim, J.W. Lee, Cone-shaped structures of GeO_2 fabricated by a thermal evaporation process, Appl. Surf. Sci. 253 (2007) 7207–7210.
[15] A.A. Bolzan, C. Fong, B.J. Kennedy, C.J. Howard, Structural studies of rutile-type metal dioxides, Acta Crystallogr. B 53 (1997) 373–380.
[16] W.H. Baur, A.A. Khan, Rutile-type compounds. IV. SiO_2, GeO_2 and a comparison with other rutile-type structures, Acta Crystallogr. B 27 (1971) 2133–2139.
[17] J. Haines, O. Cambon, E. Philippot, L. Chapon, S. Hull, A neutron diffraction study of the thermal stability of the α-quartz-type structure in germanium dioxide, J. Solid State Chem. 166 (2002) 434–441.
[18] J. Glinnemann, H.E. King, H. Schulz, T. Hahn, S.J. la Placa, F. Dacol, Crystal structures of the low-temperature quartz-type phases of SiO_2 and GeO_2 at elevated pressure, Z. Kristallogr. 198 (1992) 177–212.
[19] G.S. Smith, P.B. Isaacs, The crystal structure of quartz-like GeO_2, Acta Crystallogr. 17 (1964) 842–846.
[20] T. Yamanaka, K. Ogata, Structure refinement of GeO_2 polymorphs at high pressures and temperatures by energy-dispersive spectra of powder diffraction, J. Appl. Crystallogr. 24 (1991) 111–118.
[21] V.P Prakapenka, G. Shen, L.S. Dubrovinsky, M.L. Rivers, S.R. Sutton, High pressure induced phase transformation of SiO_2 and GeO_2: difference and similarity, J. Phys. Chem. Solids 65 (2004) 1537–1545.
[22] S.X. Wang, L.M. Wang, R.C. Ewing, Ion irradiation-induced amorphization of two GeO_2 polymorphs, Nucl. Instrum. Meth. Phys. Res. B 175–177 (2001) 615–619.
[23] S. Kalem, O. Arthursson, I. Romandic, Transformation of germanium to fluogermanates, Appl. Phys. A 98 (2010) 423–428.
[24] V.V. Atuchin, T.A. Gavrilova, S.A. Gromilov, V.G. Kostrovsky, L.D. Pokrovsky, I.B. Troitskaia, R.S. Vemuri, G. Carbajal-Franco, C.V. Ramana, Low-temperature chemical synthesis and microstructure analysis of GeO_2 crystals with α-quartz structure, Cryst. Growth Des. 9 (2009) 1829–1832.
[25] J.D. Rimer, D.D. Roth, D.G. Vlachos, R.F. Lobo, Self-assembly and phase behavior of germanium oxide nanoparticles in basic aqueous solutions, Langmuir 23 (2007) 2784–2791.
[26] N.F. Mott, E.A. Davis, Electronic Processes in Non-Crystalline Materials, 2nd ed., Clarendon, Oxford, UK, 1979.
[27] R.S. Vemuri, K. Kamala Bharathi, S.K. Gullapalli, C.V. Ramana, Effect of structure and size on the electrical properties of nanocrystalline WO_3 films, ACS Appl. Mater. Interfaces 2 (2010) 2623–2629.
[28] N.F. Mott, Conduction in glasses containing transition metal ions, J. Non-Cryst. Solids 1 (1968) 1–17.
[29] A. Yildiz, S.B. Lisesivdin, M. Kasap, D. Mardare, Non-adiabatic small polaron hopping conduction in Nb-doped TiO_2 thin film, Physica B 404 (2009) 1423–1426.